Journal of Petroleum Science and Engineering 208 (2022) 109368

Contents lists available at ScienceDirect

Journal of Petroleum Science and Engineering

journal homepage: www.elsevier.com/locate/petrol

# Improved seismic well tie by integrating variable-size window resampling with well-tie net

Hao Wu [a], Zhen Li [b], Naihao Liu [b], Bo Zhang [c,*]

[a] China University of Geosciences, School of Earth Resources, China
[b] Xi'an Jiaotong University, School of Information and Communications Engineering, China
[c] The University of Alabama, Department of Geological Science, China

ARTICLE INFO

Keywords:
Seismic well tie
Waveform resampling
CNN

ABSTRACT

Accurate seismic well tie is essential for seismic inversion and reservoir characterization. The procedure of seismic well tie involves shifting, stretching and squeezing the synthetic seismogram computed from well logs to match the seismic traces at or near the borehole location. Numerous methods have been proposed for nonlinear alignment between synthetic and real seismograms. However, most well-tie methods are prone to over-stretching and the alignment result is sensitive to the chosen window size. To solve those problems, we propose a variable-size window resampling (VWR) algorithm and integrate with convolutional neural network (CNN) for automatic seismic well tie. Using VWR algorithm to reconstruct the waveforms in synthetic seismogram can simulate the variety of subsurface velocity. CNN can learn the characteristic of different waveforms and recognize the most correlated waveforms between synthetic and real seismograms for sequence alignment. We first use VWR algorithm to reconstruct a large number of synthetic seismograms for train set generation. We then build an CNN model that named well-tie net for training to learn the feature of different resampled synthetic seismograms. Finally, we use the well trained CNN model to segment the real seismogram and align with the synthetic seismogram for seismic well tie. We apply our method into the synthetic test and real seismic data with well logs and obtain high correlated seismic-well tie. We also compare with the conventional method dynamic time warping (DTW) to illustrate the effectiveness and robustness of our proposed method. Our proposed method can avoid the problem of over-stretching by using the variable-size window resampling algorithm and automatically tying the well to seismic trace using well-tie net. In addition, the train set for our method is generated automatically.

## 1. Introduction

Tying well log to seismic trace is a key step to connect seismic data to geological property. Seismic data is commonly interpreted in the time-domain, while the well logs are recorded in the depth-domain. The time-depth function between seismic and well log is depending on the velocity. However, the velocity is nonlinear and varying with the depth, which a precise velocity model is very hard to obtain. Many authors summarized the common procedure of seismic well ties (Peterson et al., 1955; White, 1980; White, 1997; White and Simm, 2003), which includes four steps: (1) computing a reflectivity series using the velocity log and density log, (2) estimating a proper wavelet, (3) generating a synthetic seismogram through the convolution, (4) matching the synthetic seismogram with the real seismogram through shifting, stretching and squeezing.

Time consuming and possible over-stretching are the two challenges for seismic well tie. Manually tying is matching the synthetic to the real seismogram point by point, which is time consuming. Many automatic methods have been proposed to overcome this issue. White and Simm (2003) tie the well log to seismic using a window based cross correlation method, whereas it limited to linear shift features. Besides, the alignment result of window-based methods is varying with the chosen window size and the best window size is hard to determine. Nonlinear alignment methods (Muñoz and Hale, 2012; Herrera et al., 2014) have been proposed based on the dynamic time warping (DTW) (Sakoe and Chiba, 1978). However, those methods focus on better alignment result and may cause the problem of over-stretching. Herrera and van der Baan (2014) added a global constraint to keep the stretch and squeeze within reasonable bounds. Whereas, the alignment results may vary within different constrain conditions. Numerous methods (Hale, 2013; Muñoz

* Corresponding author.
E-mail addresses: wuhaogeo@gmail.com (H. Wu), zhen_li@mail.xjtu.edu.cn (Z. Li), naihao_liu@mail.xjtu.edu.cn (N. Liu), bzhang33@ua.edu (B. Zhang).

https://doi.org/10.1016/j.petrol.2021.109368
Received 9 March 2021; Received in revised form 20 July 2021; Accepted 9 August 2021
Available online 11 August 2021

and Hale, 2015) aimed to smooth the alignment result by using dynamic warping of seismic images (DIW), which set the maximum strain for each sample. Wu and Caumon (2017) proposed a DTW based method to simultaneously tie multiple wells to seismic image by flattening synthetic and corresponding real seismograms.

CNN (LeCun et al., 1998) is a computational model that composed of multiple processing layers, which can learn features of target data with different scales (LeCun et al., 2015). CNN based methods have obtained great successes in speech recognition and objects detection. Those methods for objects segmentation include AlexNet (Krizhevsky et al., 2012), Region-based convolutional neural network (RCNN) (Girshick et al., 2014), GoogleNet (Szegedy et al., 2015), VggNet (Simonyan and Zisserman, 2015), and so on. However, these methods can only recognize the target object in regional level. Fully connected convolutional neural network (FCN) (Long et al., 2015) dramatically improved the capability of objects detection from regional level to element level. He et al. (2015) proposed Residual neural network (ResNet) that adds a skip connection into CNN architecture to make training of a very deep network possible. Recently, numerous CNN based approaches have been applied into seismic interpretation (Huang et al., 2017; Di et al., 2018; Pham et al., 2018; Shi et al., 2018; Zhao and Mukhopadhyay, 2018; Wu et al., 2018, 2019a, 2019b, 2020; Liu et al., 2020) Those methods have achieved robust and effective results for seismic interpretation. However, most of these methods require the man-made label in the process of data preparation for CNN training. Manually picking training data and training label is very time consuming and the prediction result is depending on the quality of those manual training label. Wu et al. (2019c) proposed an unsupervised CNN for seismic fault detection by building millions of synthetic fault models in the training processing. Another unsupervised learning method like waveform embedding for horizon picking (Shi et al., 2020) is learning the features of nearby waveforms using fixed-size window.

Inspired by these CNN based works, we propose a two-step automatic seismic well tie method. The first step is simulating the variety subsurface velocity. In this step, we develop the variable-size window resample (VWR) algorithm to resample the synthetic seismogram. By using VWR, we can generate a lot of resampled synthetic seismograms, which have the same length with the original synthetic seismogram but different waveforms. Hence, we can use those resampled synthetic seismograms to simulate different subsurface velocity models. The second step is building an unsupervised segmentation CNN for automatic seismic well tie, which named well-tie net. In well-tie net, we use the resampled synthetic seismograms and the corresponding class labels as the training set, which do not require the manually picking labels as training data. After training process, we apply the well-trained CNN model into the real seismogram for segmentation. Finally, we can align the synthetic seismogram with real seismogram based on the segmentation boundaries.

This paper is organized as follows: We first briefly introduce the general procedure of seismic well tie. We then present our proposed waveform resampling algorithm VWR for subsurface velocity simulation. We next discuss the detail of our proposed well-tie net for automatic seismic-well tie. We finally apply it into synthetic and real data to demonstrate the robustness and effectiveness of our proposed method.

### *1.1. Conventional procedure of seismic well tie*

Seismic well tie is a procedure of matching the synthetic seismogram that computed from well logs to the real seismic trace near the borehole location (Walden and White, 1984). The common procedure of seismic well tie can be concluded into four steps. The first step is computing the reflectivity series $r(z)$ based on the velocity log $v(z)$ and density log $\rho(z)$:

$$r(z) = \frac{\rho(z+\Delta z)v(z+\Delta z) - \rho(z)v(z)}{\rho(z+\Delta z)v(z+\Delta z) + \rho(z)v(z)} \tag{1}$$

The second step is estimating an proper wavelet $w(\tau)$. The third step is calculating the synthetic seismogram $x(\tau)$ by convolving the reflectivity series with the wavelet $w(\tau)$:

$$x(\tau) = r(z)^* \, w(\tau) \tag{2}$$

where * denotes the convolution operator.

The final step is shifting, squeezing and stretching the synthetic seismogram to match the real seismic trace. Manually seismic well tie is very time-consuming to obtain a good alignment result. Many automatic seismic well tie methods have been proposed to accelerate the procedure of alignment. However, most of them cannot avoid the problem of overstretching (Hale, 2013).

### *1.2. Variable-size window resampling for subsurface velocity simulation*

The subsurface velocity is varying with depth and the time-depth function between well log and seismic trace is determined by velocity. A precise subsurface velocity model is the key factor to guarantee a reasonable seismic well tie. However, we usually can only get an approximately velocity model but not a precise one. Hence, the first part of our method for seismic well tie is reconstructing the synthetic seismogram to simulate different situations of the subsurface velocity model.We present an example to demonstrate that the length and waveform of a real seismogram are highly dependent on the variety subsurface velocity. We thus generate a synthetic seismogram with defined length and waveform (Fig. 1a), where the depth is 300 m and the sample rate is 0.5 m. To simulate the corresponding real seismogram in the time-domain, we assume the subsurface velocities are 1500 m/s, 2000 m/s and 2500 m/s, respectively. Here, we obtain three different real seismograms in Fig. 1b. Note that both the synthetic seismogram and real seismogram have a similar waveform but different lengths. Thus, we need to align the synthetic seismogram with the real seismogram to compute an accurate time-depth function.

Fig. 2 shows the workflow for reconstructed synthetic seismograms generation. The first step is well data conditioning for improving the quality of input data. The second step is extracting initial statistical wavelet only use seismic trace near borehole. The third step is computing the reflectivity from density and velocity log, then convoloving with statistical wavelet to generate the initial synthetic seismogram. The fourth step is using check shot data to estimate the initial time depth function. The fifth step is combining seismic trace and well log to extract wavelet with constant phase and update the synthetic seismogram. The sixth step is segmenting the synthetic seismogram based on the well log markers (Fig. 3). The final step is using our

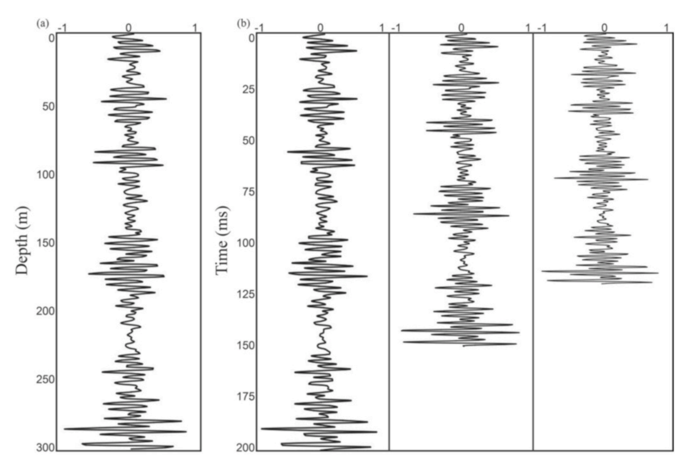


**Fig. 1.** Illustrating that the length and waveform of real seismogram highly depends on the variety of subsurface velocity models. (a) Synthetic seismogram that the depth is 300 m and the sample rate is 0.5 m. (b) Three simulated real seismograms with different subsurface velocities, which we assume the subsurface velocities are 1500 m/s, 2000 m/s, and 2500 m/s, respectively.

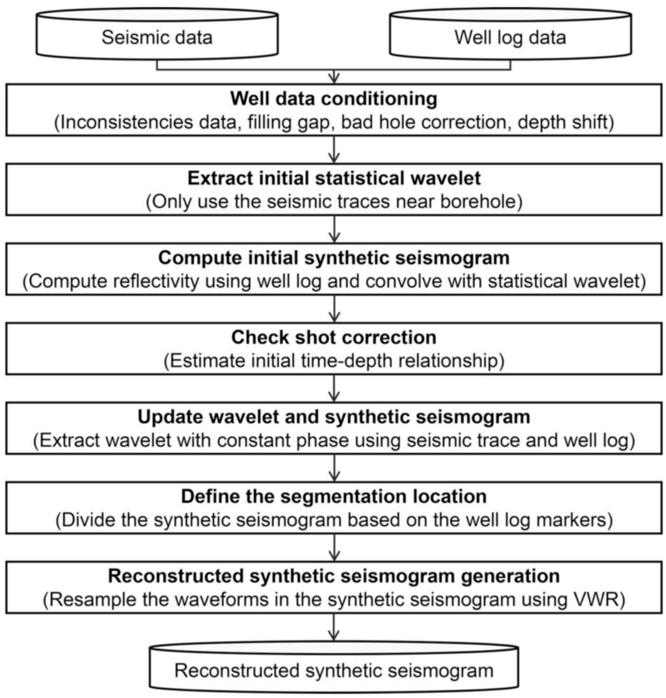


**Fig. 2.** Our proposed workflow for reconstructed synthetic seismograms generation.

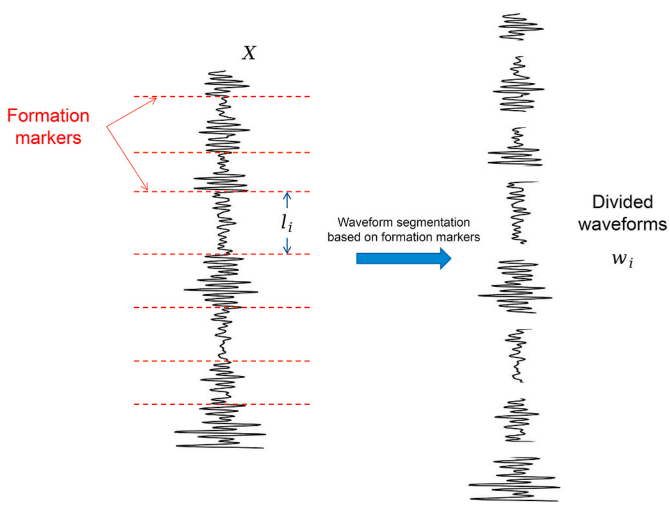


**Fig. 3.** The process that divide the synthetic seismogram based on the formation markers.

proposed variable-size window resampling (VWR) algorithm to resample the divided waveforms in synthetic seismogram and output the reconstructed synthetic seismograms.

Our proposed VWR algorithm is shown as follow:

Consider a synthetic seismogram $X$ with length $L$ has been divided into N waveforms $w_i$ based on formation markers, which the length of each waveform is $l_i$. Next, we change the length of each waveform from $l_i$ to $\widehat{l_i}$, where $\sum_{i=1}^{N} l = \sum_{i=1}^{N} \widehat{l} = L$. To avoid abnormal velocity change, we set a constraint that the shift length $s$ is range from [-10 %, 10 %] of the waveform length $l_i$. Then, we generate the resampled waveform $\widehat{w_i}$ based on the shifted waveform length $\widehat{l_i}$ (Fig. 4). Finally, we group all the resampled waveforms to generate the reconstructed synthetic seismogram $\widehat{X}$. Hence, we can use those reconstructed synthetic seismograms to simulate different subsurface velocity models.

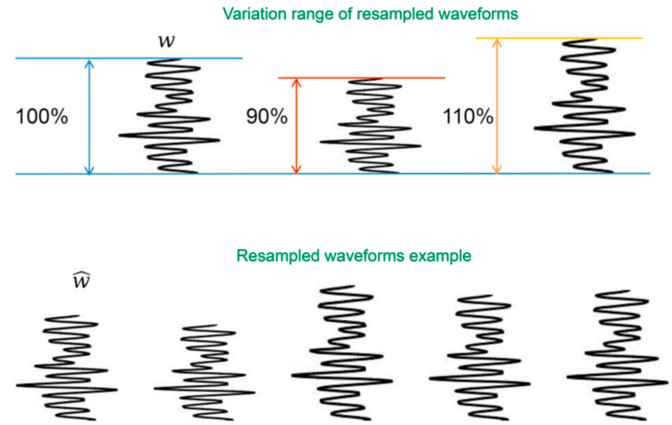


**Fig. 4.** The procedure for generating resampled synthetic seismogram. To avoid abnormal velocity change, we set a constraint that the shift length $s$ is range from [-10 %, 10 %] of the waveform length.

### 1.3. Well-tie net for automatic seismic well tie

The second part of our method is developing a CNN model (well-tie net) for automatic seismic well tie.

### 1.4. Train set generation

Train set includes train data and corresponding label. It is essential for CNN model and the quality of train set has a great influence on the prediction accuracy of CNN model.

Fig. 5 shows the workflow of train set generation. We start with producing the original class label based on the formation markers (the segments are labeled with different integer number from top to bottom). We then divide the original synthetic seismogram into several segmented waveforms based on the formation markers. Next, we apply VWR algorithm to resample each segmented waveform and produce the updated label. We finally connect all the resampled waveforms and updated labels to generate the reconstructed synthetic waveforms and corresponding labels. VWR algorithm can produce a large number of variable train set at one time, which meet the requirement of train set for CNN model. Fig. 6a shows five representative reconstructed synthetic seismograms and Fig. 6b shows the corresponding labels. Note that the varying characteristic of waveforms and labels in those reconstructed synthetic seismograms.

### 1.5. Well-tie net

After train set preparation, the next step is building an CNN model to learn the characteristic of different waveforms. Fig. 7 shows the architecture of our proposed well-tie net.

The CNN model contains two main parts: encoder and decoder, which consist of a sequence of nonlinear processing layers and followed by a classification layer. The role of the encoder is transforming the input data into feature maps and capturing its effective information. The encoder contains a series of nonlinear processing layers and each layer contains convolution filters, batch-normalization regularizer (BN) (Ioffe and Szegedy, 2015), rectified linear units (ReLU) activation operator and max-pooling operator. The objective of the convolution filter is extracting the feature of input waveforms to form the feature maps. The equation of the convolution filter is shown as:

$$O = \mathrm{b} + f * \mathrm{z}, \tag{3}$$

Where * denotes the convolution operation, b denotes the bias term, z is

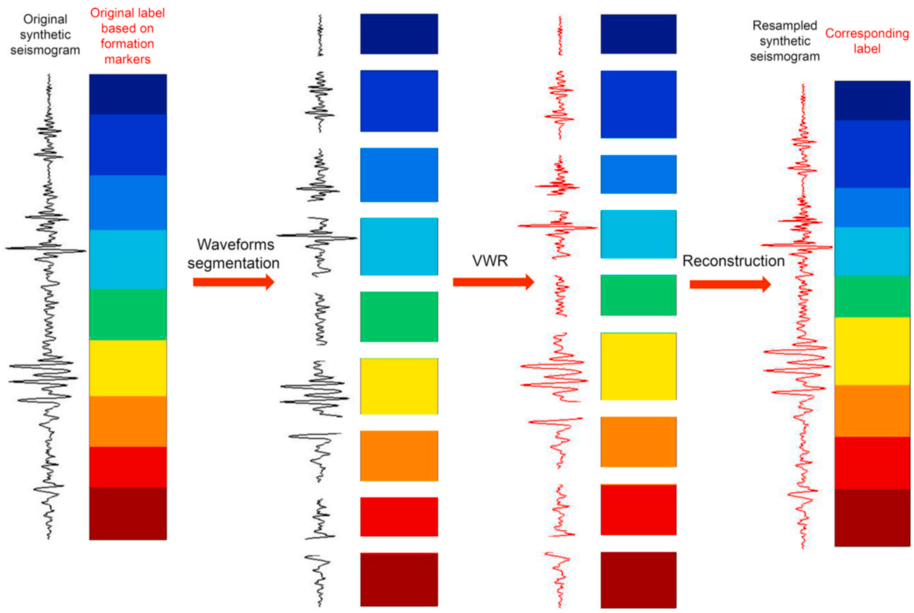


**Fig. 5.** The workflow of train set generation. We start with producing the original class label based on the formation markers (the segments are labeled with different integer number from top to bottom). We then divide the original synthetic seismogram into several segmented waveforms based on the formation markers. Next, we apply VWR algorithm to resample each segmented waveform and produce the updated label. We finally connect all the resampled waveforms and updated labels to generate the reconstructed synthetic waveforms and corresponding labels.

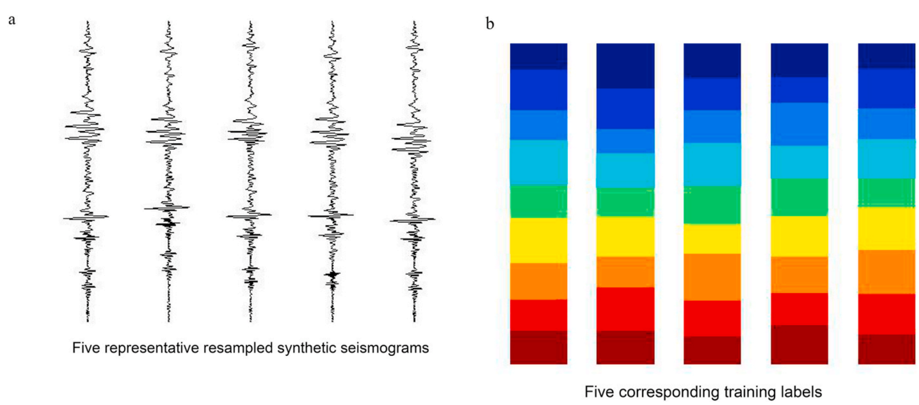


**Fig. 6.** The resampled synthetic seismograms and corresponding class label. (a) Five representative resampled synthetic seismograms. (b) The corresponding training labels.

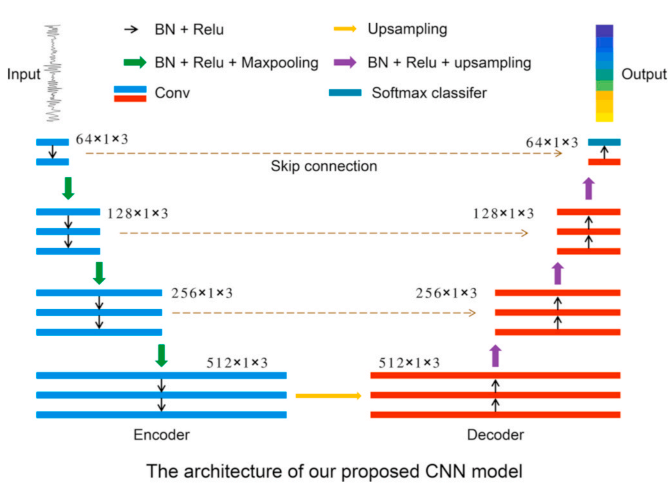


**Fig. 7.** The architecture of our proposed CNN model for automatic seismic well tie.

the input waveforms, $f$ is the convolution filter, and $O$ is the output feature map. With the max-pooling operator, the encoder down-samples the feature maps and learns the features of waveforms with different scales. Then, the encoder transfer the feature maps to the decoder.

Different from the encoder, the decoder contains an up-sampling operator in its processing layers. The role of the decoder is reconstructing feature maps and constructing the relationship between the input data and target labels. In this paper, the encoder and decoder show a symmetric architecture and the decoder will reconstruct the feature maps and figure out the relationship between the waveforms (training data) and target locations (class labels). Finally, we use a softmax classifier to give each waveform sample with the probabilities for each label.

### 1.6. Automatic seismic well tie using well-tie net

The final step of our method is training the proposed CNN model using reconstructed synthetic seismograms and testing in the real seismogram. Fig. 8 shows the workflow of training and testing process. We feed the resampled synthetic seismograms and corresponding labels into CNN model for training. In the training process, our CNN model achieves the converge state after 20 epochs and the accuracy is larger than 99 %. As a result, we apply the well-trained CNN model into the real seismogram for segmentation and output the class label. Then, we can align the

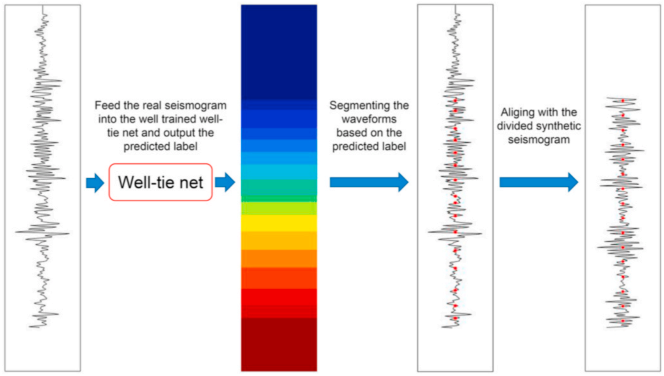


**Fig. 8.** The workflow of training and testing process.

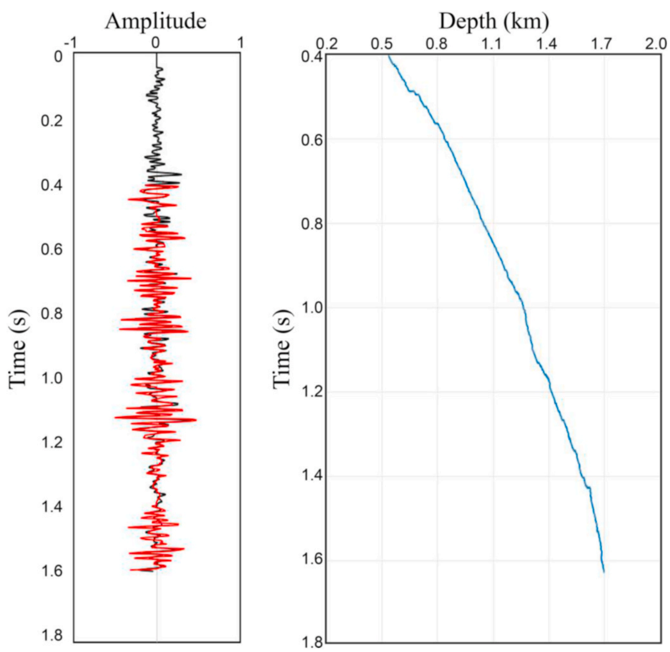


**Fig. 9.** The aligned synthetic seismogram with the real seismogram and the corresponding time-depth function.

synthetic seismogram with the real seismogram and compute the time-depth function based on these segmented waveforms (Fig. 9).

### 1.7. Applications

To evaluate the performance of our proposed method for automatic seismic well tie, we apply our method to synthetic data and real data.

### 1.8. Synthetic test

Consider two synthetic seismograms $f(t)$ and $g(t)$ with length N = 128 samples displayed in Fig. 10. The shift function $s(t) = f(t) - g(t)$between these two synthetic seismograms is a sinusoidal function. According to this sinusoidal function, the shift range between two adjacent points $|e(t) = s(t+1) - s(t)| < 1$. In other words, the situation of 100 % stretching or squeezing would not happen, which can avoid the abnormal velocity change.

Since there is no formation markers for these synthetic seismograms, we first segment the synthetic seismogram $f(t)$ with a fixed-size window and generate corresponding label. We then use VWR algorithm to generate the reconstructed synthetic seismograms for train set preparation. The size of the resampling window is range from 4 to 12 and the

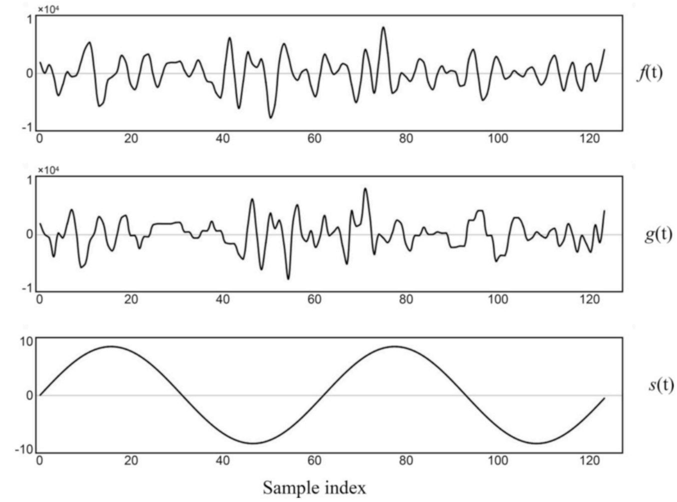


**Fig. 10.** Two synthetic seismograms f(t) (first line) and g(t) (second line) with the known sinusoidal equation shifts (third line).

volume of reconstructed synthetic seismograms is 10000. We use 30 % of the reconstructed synthetic seismograms as train set and apply the rest of 70 % data into blind test to validate our CNN model. During the training process our CNN model is converged after 20 epochs and the training accuracy is greater than 99 % and the test accuacy is over 93 %. Then, we apply the well-trained model into the synthetic seismogram $g(t)$ to segment the best matching waveforms. Finally, we align these two sequences and computing the shift function between $f(t)$ and $g(t)$ based on the segmented waveforms. Fig. 11 shows the alignment result and the comparison between the true shift function and the shift function using our proposed method. Note that our CNN model have recognized the best matching waveforms between $f(t)$ and $g(t)$. We compare our computed shift function with the original shift function, which shows a very good match result.

### 1.9. Real data test

We apply our proposed method into two different field examples. The first field example is from the open source data F3-block including 3D post-stack seismic data and four wells (Fig. 12). In this work, we choose two wells to evaluate the performance of our proposed method and compare with the conventional method DTW.

To automatically tying well logs with seismic traces near the borehole location, we begin by computing the synthetic seismogram from well F03-2. We first follow the process of reconstructed synthetic seis-

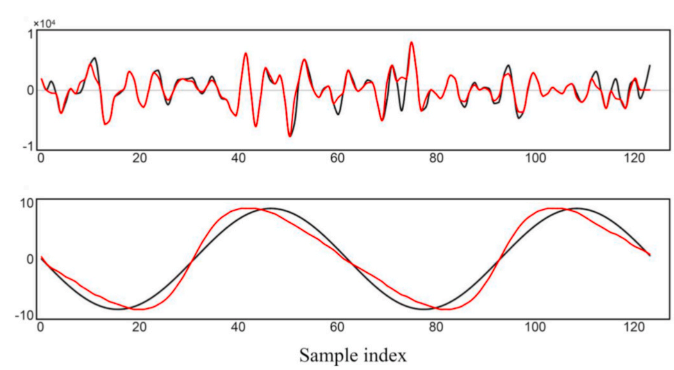


**Fig. 11.** The alignment result between f(t) and g(t) (first line), the comparison between true shift function (black) and the shift function computed by using our proposed method (red). (For interpretation of the references to colour in this figure legend, the reader is referred to the Web version of this article.)

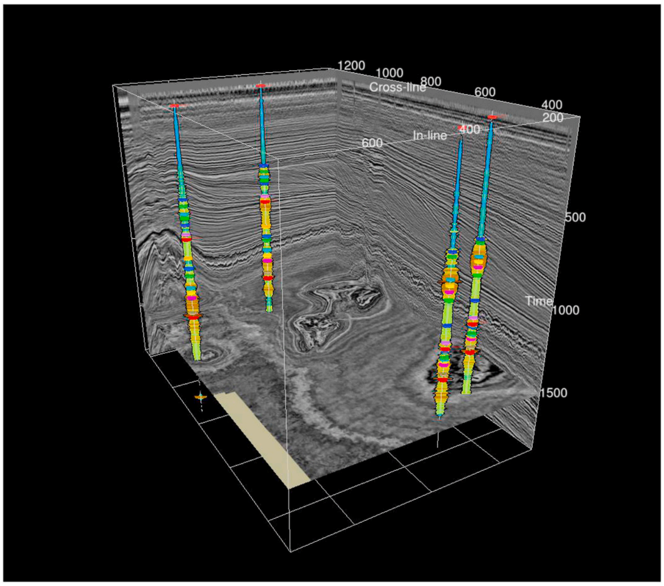


**Fig. 12.** The survey of the first field example. This survey is from the open source data F3-block that include 3D post-stack seismic data and four wells.

mograms generation workflow in Fig. 2 to extract the wavelet. Fig. 13a and c shows our extracted initial statistical wavelet and contant phase wavelet by using seismic data and well log, which Fig. 13b and d shows the corresponded amplitude spectrum and phase. We then convolve the constant phase wavelet with the reflectivity to generate the synthetic seismograms $X$using equation (2). As shown in Fig. 14a, the synthetic seismogram (red) computed based on well logs do not match seismic traces (black).

Next, we follow the procedure in Fig. 5 to generate the train set. We segment the synthetic seismograms $X$based on the formation markers and generate the corresponding class labels with different numbers from top to bottom. We then resample the synthetic seismograms using VWR. The shift difference between the resampling windows and original segementation window is range from −10 % to 10 %. Thus, the reconstructed synthetic seismograms and corresponding labels are treated as train set for the following CNN based automatic seismic well tie. The total number of train set is 100000.

To apply our proposed CNN model aligning the synthetic seismogram with seismic traces, we first feed the training set into our CNN model. Our CNN model meets a converge state after 50 epochs. Both the training accuracy and validation accuracy exceed 97 %. Afterward, we apply the well-trained model into real seismogram to pick the most correlated waveforms and segment the sequence. Fig. 14b shows the alignment result using well-tie net. In comparison, we use DTW to illustrate the robustness of our proposed method. Fig. 14c shows the alignment result using DTW. Note the zoom view in blue box and green box that our proposed method shows a very good matching and smooth result between the real seismogram and synthetic seismogram. Whereas, the alignment result using DTW contains several over-stretching parts indicate by green arrows in green box.

We also compute the time-depth function and interval velocity difference to validate the robustness of our proposed method and compare with DTW. Fig. 15a shows the initial time-depth function (black curve), final time-depth function (red curve) calculating by using well-tie net and final time-depth function computed by using DTW (green curve). After detailed comparisons, our method shows a very smooth result and does not show any rapid change in the time-depth function. In contrast, we observe the unpractical big shift between the initial time-depth function and final time-depth function computed by using DTW. Besides, Fig. 15b shows the initial interval velocity (black curve), interval velocity using well tie net (red curve) and interval velocity using DTW (green curve). From Fig. 15c we can see that the interval velocity difference by using well-tie net is smaller than 10 %, while the velocity difference by using DTW have shown the abnormal velocity change indicated by blue arrows.

Fig. 16 shows another field example using well F03-4. We first compute the synthetic seismogram using the density log and velocity log. We then estimate the initial time-depth function using the velocity log. As shown in Fig. 16a, the synthetic seismogram (red curve) computed with the initial time-depth function does not match the real seismogram (black curve). Next, we repeat the procedure for well F03-2 to match the synthetic seismogram with the real seismogram shown in Fig. 16b. We use DTW as the comparison method to align these

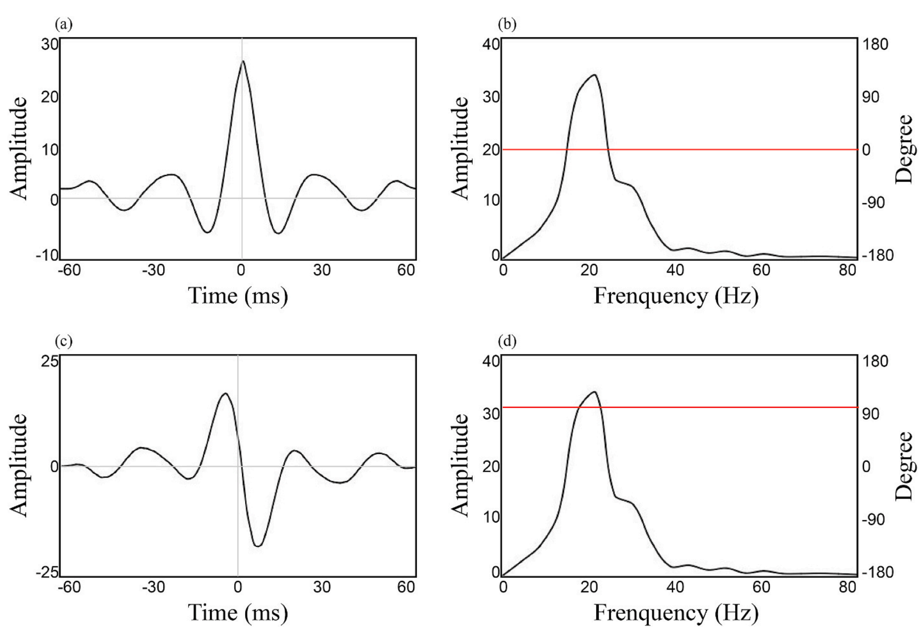


**Fig. 13.** The extracted wavelet and spectrum for computing the synthetic seismogram. (a) the extracted initial statistical wavelet. (b) the amplitude and phase spectrum that correspond to the initial statistical wavelet. (c) the extracted constant phase wavelet after check shot correction. (d) the amplitude and phase spectrum that correspond to the constant phase wavelet.

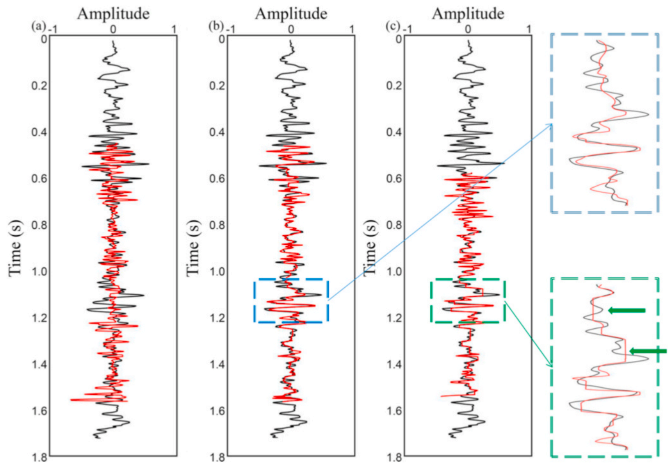

**Fig. 14.** The seismic-well tie result of the first field example well F03-2. (a) The aligned synthetic seismogram (red) and real seismogram (black) using initial time-depth function. (b) The aligned synthetic seismogram (red) and real seismogram (black) using well-tie net. (c) The aligned synthetic seismogram (red) and real seismogram (black) using DTW. Note the zoom view (blue and green boxes) over-stretching area indicate by green arrows. (For interpretation of the references to colour in this figure legend, the reader is referred to the Web version of this article.)

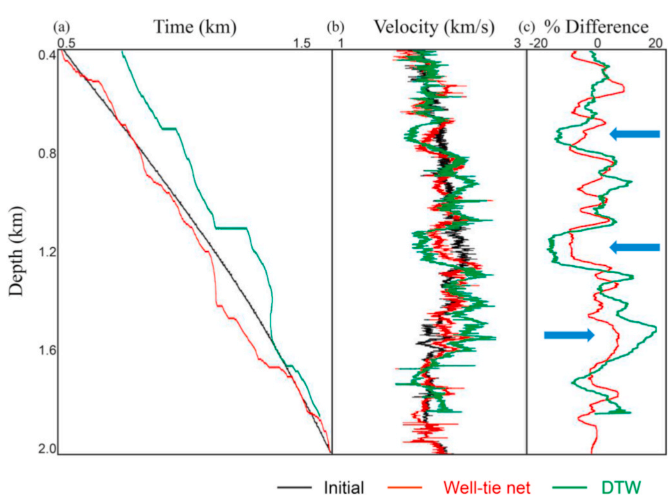

**Fig. 15.** (a) the comparison of time-depth function among the original (black), well-tie net (red) and DTW (green) in the well F03-2. (b) the comparison of interval velocity among the original (black), well-tie net (red) and DTW (green). (c) the comparison of interval velocity difference between the well-tie net (red) and DTW (green). Note that the interval velocity difference by using well-tie net is smaller than 10 %, while the velocity difference by using DTW have shown the abnormal velocity change indicated by blue arrows. (For interpretation of the references to colour in this figure legend, the reader is referred to the Web version of this article.)

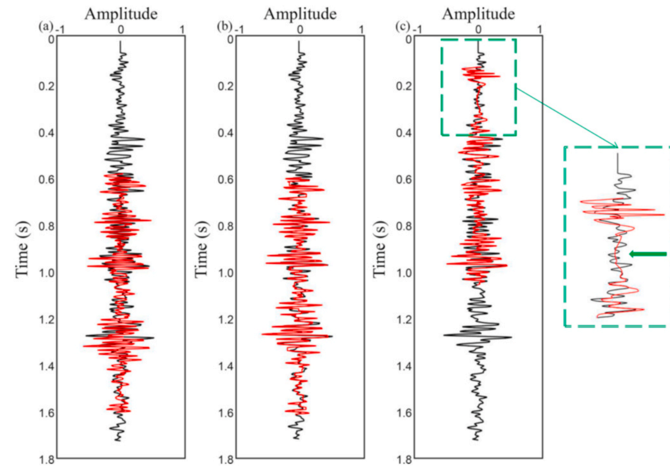

**Fig. 16.** The seismic-well tie result of the second field example well F03-4. (a) The aligned synthetic seismogram (red) and real seismogram (black) using initial time-depth function. (b) The aligned synthetic seismogram (red) and real seismogram (black) using well-tie net. (c) The aligned synthetic seismogram (red) and real seismogram (black) using DTW. Note the zoom view (blue and green boxes) over-stretching area indicate by green arrows. (For interpretation of the references to colour in this figure legend, the reader is referred to the Web version of this article.)

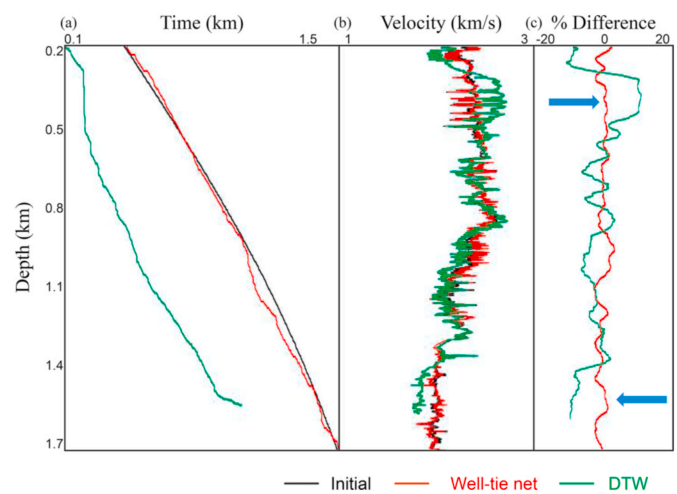

**Fig. 17.** (a) the comparison of time-depth function among the original (black), well-tie net (red) and DTW (green) in well F03-4. (b) the comparison of interval velocity among the original (black), well-tie net (red) and DTW (green). (c) the comparison of interval velocity difference between the well-tie net (red) and DTW (green). Note that the interval velocity difference by using well-tie net is smaller than 10 %, while the velocity difference by using DTW have shown the abnormal velocity change indicated by blue arrows. (For interpretation of the references to colour in this figure legend, the reader is referred to the Web version of this article.)

seismograms. We observe the alignment result using our proposed method (Fig. 16b) is matched very well. However, the aligned synthetic seismogram using DTW (Fig. 16c) shows significant differences with the original synthetic seismogram, which displayed in the zoom view of green box indicated by green arrows. We also compute the time-depth function to illustrate the robustness of our proposed method and compare with DTW. As shown in Fig. 17a, the initial time-depth function (black curve) is almost same with the final time-depth function computed by using well-tie net (red curve) but shows significant difference with DTW (green curve). Besides, Fig. 17b shows the initial interval velocity (black curve), interval velocity using well tie net (red curve) and interval velocity using DTW (green curve). From Fig. 17c we can see that the interval velocity difference by using well-tie net is smaller than 10 %, while the velocity difference by using DTW have shown the abnormal velocity change indicated by blue arrows.

The second field example is the well JV37 that located in Oklahoma, US. We also follow the procedure for the frist field example to align the synthetic seismogram with real seismogram using well-tie net and DTW, respectively (Fig. 18). We observe the alignment result using our proposed method (Fig. 18b) is matched very well. However, the aligned synthetic seismogram using DTW (Fig. 18c) shows significant differences with the original synthetic seismogram, which displayed in the zoom view of green box indicated by green arrows. Thus, we can

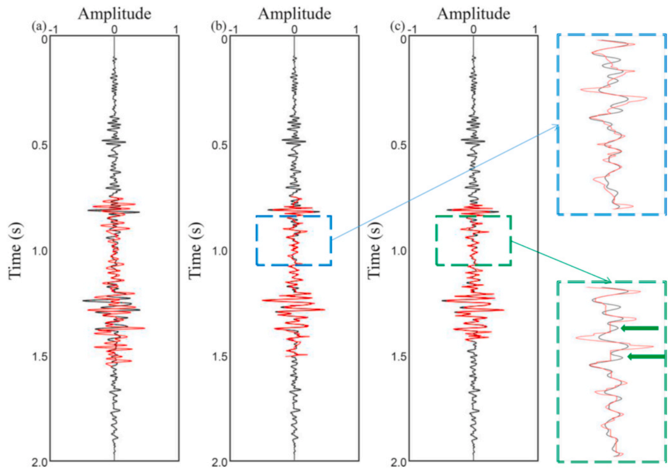


**Fig. 18.** The seismic-well tie result of the second field example well JV37. (a) The aligned synthetic seismogram (red) and real seismogram (black) using initial time-depth function. (b) The aligned synthetic seismogram (red) and real seismogram (black) using well-tie net. (c) The aligned synthetic seismogram (red) and real seismogram (black) using DTW. We observe the alignment result using our proposed method (Fig. 18b) is matched very well. However, the aligned synthetic seismogram using DTW (Fig. 18c) shows significant differences with the original synthetic seismogram, which displayed in the zoom view of green box indicated by green arrows. (For interpretation of the references to colour in this figure legend, the reader is referred to the Web version of this article.)

conclude that our proposed method for automatic seismic well tie can not only obtain an accurate alignment result but also avoid the problem of over-stretching.

### *1.10. Disscussion*

The number of train set is a key factor affecting the performance of CNN model. We have designed an experiment to test the prediction accuracy of CNN model by applying different train set volume. We set the number of reconstructed synthetic seismograms are 100, 500, 1000, 2000 and 5000, respectively. The corresponding test accuracy are 44.3 %, 71.6 %, 91.2 %, 93.1 % and 93.3 %, respectively. This experiment result indicate that if the train set number is over 1000, our proposed well-tie net can avoid the problem of overfiting and get a satisfied well-tie result.

Besides, we believe the stretching range of variable size window is also a key influence factor to the train set quality. Larger shift range can simulate more subsurface velocity models, while it would cause abnormal velocity change. To achieve a reasonable seismic well tie result, we set the variable size windows are shifting range from −10 % to 10 %.

## 2. Conclusions

We propose a two-step automatic seismic well tie method. Our method first simulates the variety subsurface velocity. We then use CNN model to learn the features of different waveforms and tie the well to seismic automatically.

To simulate the variety subsurface velocity, we present a variable-size window resampling (VWR) algorithm to resample the synthetic seismogram. By generating a large number of different resampled synthetic seismograms, we can simulate different situations of subsurface velocity models. To learn the characteristic of different resampled synthetic seismogram, we propose an unsupervised segmentation CNN model, which named well-tie net. We use well-tie net to learn the features of waveforms and output the corresponding class labels. With those class labels, we can segment the real seismogram and align with the synthetic seismogram according to the segmentation boundaries.

The problem of over-stretching is often caused by the point-to-point alignment. This kind of methods are usually focus on the high correlation matching but ignore the waveform similarity. Although the window-based alignment method is aligning the sequences by matching the similar waveform, the alignment result is varying with the chosen window size. Our proposed VWR algorithm using a variable-size window can not only obtain high correlation alignment result, but also avoid the problem of over-stretching. In addition, the well-tie net is using the resampled synthetic seismograms and corresponding training labels as the training set, which do not require the manually picked labels.

## Credit author statement

Hao Wu: Conceptualization, Methodology, Programming, Software, Writing. Zhen Li: Methodolgy. Naihao Liu: Investigation. Bo Zhang: Supervision.

## Declaration of competing interest

We declare that we have no financial and personal relationships with other people or organizations that can inappropriately influence our work, there is no professional or other personal interest of any nature or kind in any product, service and/or company that could be construed as influencing the position presented in, or the review of, the manuscript entitled.

## Acknowledgement

This research was supported in part by the National Natural Science Foundation of China under Grant 41904102.

## References

Di, H., shafiq, M., AlRegib, G., 2018. Patch-level Mlp Classification for Improved Fault Detection: 88th Annual International Meeting. SEG, Expanded Abstracts, pp. 2211–2215.
Girshick, R., Donahue, J., Darrell, T., Malik, J., 2014. Rich feature hierarchies for accurate object detection and semantic segmentation. IEEE Conference on Computer Vision Pattern Recognition 580–587.
Hale, D., 2013. Dynamic warping of seismic images. Geophysics 78 (2). S105–S115.
He, K., Zhang, X., Ren, S., Sun, J., 2015. Deep residual learning for image recognition. IEEE Conference on Computer Vision Pattern Recognition 770–778.
Herrera, R.H., Fomel, S., van der Baan, M., 2014. Automatic approaches for seismic to well tying. Interpretation 2 (2). SD9-SD17.
Herrera, R.H., van der Baan, M., 2014. A semiautomatic method to tie well logs to seismic data. Geophysics 79 (3), V47–V54.
Huang, L., Dong, X., Clee, T.E., 2017. A scalable deep learning platform for identifying geologic features from seismic attributes. Lead. Edge 36, 249–256.
Ioffe, S., Szegedy, C., 2015. Batch normalization: accelerating deep network training by reducing internal covariate shift arXiv: 1502.03167.
Krizhevsky, A., Sutskever, I., Hinton, G., 2012. Imagenet classification with deep convolutional neural network. Adv. Neural Inf. Process. Syst. 27, 1090–1098.
LeCun, Y., Bottou, L., Bengio, Y., Haffner, P., 1998. Gradient-based learning applied to document recognition. Proc. IEEE 86 (11), 2278–2324.
LeCun, Y., Bengio, Y., Hinton, G., 2015. Deep learning. Nature 521, 436–444.
Long, J., Shelhamer, E., Darrell, T., 2015. Fully convolutional networks for semantic segmentation. IEEE Conference on Computer Vision Pattern Recognition 3431–3440.
Liu, N., He, T., Tian, Y., Wu, B., Gao, J., Xu, Z., 2020. Common-azimuth seismic data fault analysis using residual. UNet: Interpretation 8 (3), SM25–SM37.
Muñoz, A., Hale, D., 2012. Automatically Tying Well Logs to Seismic Data. CWP-725.
Muñoz, A., Hale, D., 2015. Automatic simultaneous multiple well ties. Geophysics 80 (5). IM45–IM51.
Peterson, R.A., Fillippone, W.R., Coker, F.B., 1955. The synthesis of seismograms from well log data. Geophysics 20 (3), 516–538.
Pham, N., Fomel, S., Dunlap, D., 2018. Automatic Channel Detection Using Deep Learning. SEG Technical Program Expanded Abstracts, pp. 2026–2029.
Sakoe, H., Chiba, S., 1978. Dynamic programming algorithm optimization for spoken word recognition. IEEE Trans. Acoust. Speech Signal Process. 26 (1), 43–49.
Shi, Y., Wu, X., Fomel, S., 2018. Automatic Salt-Body Classification Using a Deep Convolutional Neural Network. SEG Technical Program Expanded Abstracts, pp. 1971–1975.
Shi, Y., Wu, X., Fomel, S., 2020. Waveform embedding: automatic horizon picking with unsupervised deep learning. Geophysics 85 (4), WA67–WA76.

Simonyan, K., Zisserman, A., 2015. Very Deep Convolutional Networks for Large-Scale Image Recognition arXiv: 1409.1556.
Szegedy, C., Liu, W., Jia, Y., Sermanet, P., Reed, S., Auguelov, D., Erhan, D., Vanhoucke, V., Rabinovich, A., 2015. Going Deeper with Convolutions arXiv :1409.4842.
Walden, A.T., White, R.E., 1984. On errors of fit and accuracy in matching synthetic seismograms and seismic traces. Geophys. Prospect. 32 (5), 871–891.
White, R.E., 1980. Partial coherency matching of synthetic seismograms with seismic traces. Geophys. Prospect. 28 (3), 333–358.
White, R., Hu, T., 1997. How accurate can a well tie be? SEG Expanded Abstracts 16, 816.
White, R., Simm, R., 2003. Tutorial: good practice in well ties. EAGE first break 21, 75–83.
Wu, H., Zhang, B., Li, F., Liu, N., 2019a. Semiautomatic first-arrival picking of microseismic events by using the pixel-wise convolutional image segmentation method. Geophysics 84 (3). V143–V155.
Wu, H., Zhang, B., Lin, T., Cao, D., Lou, Y., 2019b. Semiautomated seismic horizon interpretation using the encoder-decoder convolutional neural network. Geophysics 84 (6), B403–B417.
Wu, X., Caumon, G., 2017. Simultaneous multiple well-seismic ties using flattened synthetic and real seismograms. Geophysics 82 (1). IM13–IM20.
Wu, X., Luming, L., Shi, Y., Fomel, S., 2019c. FaultSeg3D: using synthetic datasets to train an end to-end convolutional neural network for 3D seismic fault segmentation. Geophysics 84 (3). IM35–IM45.
Wu, X., Shi, Y., Fomel, S., Luming, L., 2018. Convolutional Neural Networks for Fault Interpretation in Seismic Images, 88$^{th}$ Annual International Meeting. SEG, Expanded Abstracts, pp. 1946–1950.
Wu, X., Geng, Z., Shi, Y., Pham, N., Fomel, S., Caumon, G., 2020. Building realistic structure models to train convolutional neural networks for seismic structural interpretation. Geophysics 85 (4), WA27–WA39.
Zhao, T., Mukhopadhyay, P., 2018. A Fault-Detection Workflow Using Deep Learning and Image Processing, 88th Annual International Meeting. SEG, Expanded Abstracts, pp. 1966–1970.